ECO-FRIENDLY REMANUFACTURING OF METALLIC SURFACES VIA ADVANCED LASER PROCESSING

Fazlay Rubbi[1], M. Merajul Haque[1], Liuyin Wang[3], Beiwen Li[2], Yantao Shen[3], Gül E Kremer[4], Yiliang Liao[1, *]

[1]*Department of Industrial and Manufacturing Systems Engineering, Iowa State University, Ames, IA 50011, USA*

[2]*School of Environmental, Civil, Agricultural and Mechanical Engineering, University of Georgia, Athens, GA 30602, USA*

[3]*Department of Electrical and Biomedical Engineering, University of Nevada Reno, Reno, NV 89557, USA*

[4]*School of Engineering, University of Dayton, Dayton, OH 45469, USA*

[*]*Corresponding Author: Yiliang Liao, leonl@iastate.edu*

1. Abstract

Remanufacturing technologies that can effectively remove surface corrosion and/or coatings while restoring surface integrity are essential for various metallic components. However, the current corrosion and coating removal strategy, which relies on a two-step "burning + blasting" process, faces significant technical and economic barriers. These include 1) the energy- and time-intensive volumetric heating step, which burns fossil fuels and causes undesirable microstructural and property changes in the component's interior; and 2) the blasting step, which leads to material waste, surface wear, and contamination issues. Therefore, it remains a grand challenge to develop an energy-efficient and eco-friendly strategy to realize effective removal of corrosion and coatings for metallic surface remanufacturing. In this study, we explored the potential of laser surface ablation as an effective surface remanufacturing technology for the removal of corrosion and coating layers, aiming to restore surface integrity. A laboratory-scale laser surface remanufacturing system was developed. The cast iron samples were machined from a used engine cylinder head for laser remanufacturing experiments. The study examined the effects of key parameters, including laser intensity and overlapping ratio. Moreover, robotic mirror reflective laser scanning control system was developed, aiming to evaluate the capability of laser remanufacturing of both external and internal surfaces of engineering components. The proposed laser processing technology is expected to provide an eco-friendly, energy-efficient, highly controllable, and user-friendly solution for metallic surface remanufacturing.

2. Introduction and Motivation

The remanufacturing and repair of metallic surfaces have become important to a variety of industries, including automotive, aerospace, military, and energy infrastructure. In particular, technologies capable of efficiently removing surface corrosion and coatings while restoring or preserving surface integrity are essential for a wide range of engineering components, such as cylinder blocks, cylinder heads, and exhaust manifolds. These technologies not only enhance the performance and longevity of components but also help reduce the environmental impact of industrial operations. The conventional techniques rely on strategy integrating burning and blasting processes for corrosion/rust and coating/paint removal. However, these techniques present several technical and environmental barriers, for instance the burning process requires volumetric heating of fossil fuels, which is high energy and time consuming. In addition, burning a heat-sensitive metal component to elevated temperatures can often lead to undesired microstructural alterations and degradation in mechanical properties [1]. On the other hand, the blasting process often causes excessive material removal, surface wear and contamination of abrasive particles employed in the process[2, 3]. Furthermore, traditional coating removal techniques involving abrasive blasting, can deteriorate the anti-corrosive properties of metallic surfaces and thereby require additional post-treatment processes. Given these limitations, developing an effective and eco-friendly remanufacturing technique to repair corroded metal surfaces remains as a crucial challenge to address.

In this project, we propose an effective solution using advanced laser surface ablation technologies to realize effective remanufacturing and repair of metallic surfaces. A laboratory-scale laser surface remanufacturing system was developed for the experiments. The cast iron samples were machined from a used engine cylinder head for laser remanufacturing experiments. The study examined the effects of key parameters, including laser intensity, scanning velocity, and scanning cycles. Moreover, robotic mirror reflective laser scanning control system was developed, aiming to evaluate the capability of laser remanufacturing of both external and internal surfaces of engineering components. This REMADE project was conducted through collaboration among researchers from multiple universities and engineers from the industry partner Volvo.

3. Current State of the Technology Industry Uses

In recent years, laser ablation process has been utilized as a non-contact, precise and eco-friendly alternative to conventional methods. Unlike traditional "burning" and "blasting" processes, laser ablation technique is capable of selective material removal with minimal mechanical stress and material loss. These useful features of this technique have made it suitable across aerospace and automotive industries, where longevity and structural integrity of the components are critical [4, 5]. However, the existing laser ablation techniques face several challenges such as optimizing processing parameters, energy input and induced thermal effects during the interaction of high intensity laser on substrate material. These limitations highlight the urgent need for an innovative, energy-efficient, and environmentally friendly method with optimized processing parameters to remove corrosion and coating while maintaining the structural integrity of the metallic surfaces.

4. Technology Approach

4.1 Experimental set-up

In the experimental phase of this research, we utilized a nano-second pulsed laser system to deliver laser energy with a wavelength of 1064 nm and a pulse width of 5 ns. The laser beam was directed using reflective mirrors and a focus lens. The target part was placed on a computer-controlled precision stage. When the target material interacted with the laser beam, it was rapidly vaporized and ionized because of the absorption of laser energy, leading to the removal of material [6-8]. The experimental set-up is illustrated in **Fig. 1**. The experiments were performed in ambient conditions without any post processing. To optimize the efficiency of the ablation process, a parametric study was conducted with focuses on laser parameters, including laser intensity, overlapping ratio (OR), and scanning cycles. To remanufacture the corroded cast iron specimens, we first categorized them into three classes based on their as-received corrosion levels: light, mild, and severe corroded conditions. Moreover, the parts with surface coatings were subjected to laser processing to identify optimal processing conditions for efficient coating removal. Surface properties, including roughness and oxidation, were measured alongside ablation depth to assess the surface integrity. The primary parameters used in this study include laser intensity and OR, which are critical for optimizing the laser ablation process. Laser intensity values were set at 0.2, 0.4, or 0.6 GW/cm², while OR values were varied across 25%, 50%, or 75%.

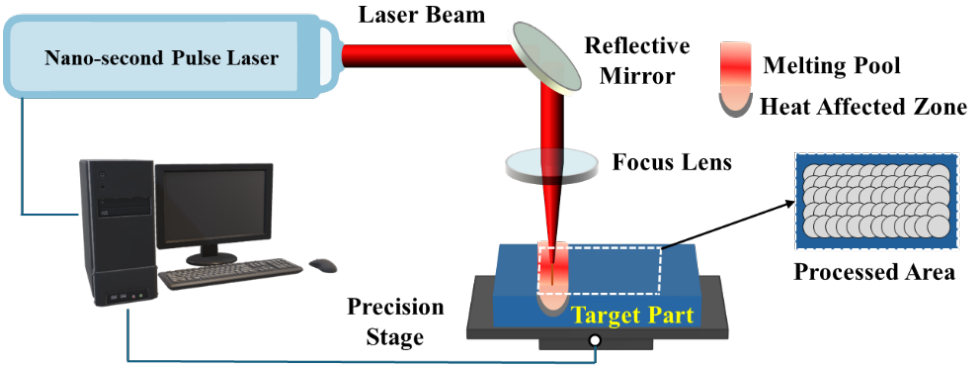

Fig. 1: Schematic illustration of the experimental set-up of laser surface remanufacturing system.

4.2 Method for inspection

Before laser remanufacturing experiments, a quantitative MATLAB-based approach was applied to assess the corrosion level of samples by analyzing their surface color characteristics in comparison with a fully corroded (100% corrosion) reference sample. High-resolution digital images of sample surfaces were captured under consistent lighting and imaging conditions to ensure accuracy. To ensure precise color analysis, the images were converted from the standard RGB (Red-Green-Blue) color space to the CIE LAB (Lightness, Green-Red, Blue-Yellow) color space using MATLAB's makecform and applycform functions. The LAB color space was chosen for its ability to represent color differences in a manner consistent with human visual perception, as exhibited in previous studies [9, 10]. Each image was decomposed into three distinct channels: L (lightness), A (green-red axis), and B (blue-yellow axis). This conversion allowed for an accurate quantification of color variations between the samples.

The fully corroded sample image was analyzed to determine its average LAB values ($L_{corroded}$, $A_{corroded}$, $B_{corroded}$). These values defined the color intensity of the fully corroded surface. The maximum possible color difference was calculated as the Euclidean distance from the LAB origin (0,0,0) to the corroded sample's average LAB values [11]. This maximum difference served as the normalization factor for further analysis, providing a reference against which the processed sample's color changes were evaluated. On the other hand, the laser-processed samples were analyzed similarly to determine its average LAB color values. The Euclidean distance between the LAB values of the fully corroded sample and the processed sample was calculated to measure the extent of color change after laser processing. This distance reflected the reduction in visible corrosion achieved through laser remanufacturing. Furthermore, the corrosion levels of samples were expressed as a percentage by normalizing the color difference with the maximum possible color difference. This calculation provided a quantitative measure of the residual corrosion on the laser-processed surface, as: $Corrosion\ level\ (\%) = \frac{Color\ difference}{Maximum\ color\ difference} \times 100\%$. The entire analysis process was implemented in MATLAB.

4.3. Robotic mirror reflective laser scanning control system

Standard laser ablation systems often face challenges in effectively removing corrosion and coating from complex cavities due to intricate geometries, large sizes, and limited motion freedom, which hinder the laser beam's ability to reach all areas of the target surface, particularly the internal surfaces [12]. To address these challenges, a novel, lightweight, miniaturized robotic mirror reflective laser scanning control system was proposed and successfully developed. This system consisted of a compact, innovative 3D gimbal mechanism, an image transmission module, a reflective mirror, and a base station. The 3D gimbal mechanism included two MKS DS75K motors, 3D-printed connectors, and a hollow metal telescopic rod. The entire mechanism weighed only 42.4 grams, with an end-effector volume of 23.7 cm² and a mirror rotation angle precision of 0.046°. The image transmission module relayed real-time images of the internal surface of the Volvo engine block cavity to the base station, which then analyzed the distribution of rust layers. Based on this analysis, the base station controlled the 3D gimbal mechanism to adjust the mirror's angle, reflect the laser beam, and efficiently remove corrosion and coating from the affected areas.

The mechanism, setup, and operation diagrams of the proposed robotic mirror reflective laser scanning control system are presented in **Fig. 2**. In **Fig. 2d**, a laser beam emitted from the laser diode at the top of the cavity is directed toward the mirror for reflection. The system is positioned within the cavity using a metal telescopic tube, as shown in **Fig. 2b**. This setup allows for real-time imaging and analysis of the rusted area for laser scanning, as illustrated in **Fig. 2e**, where the scanning pattern can be selected and adjusted accordingly. After assessing the internal cavity surface image based on rust conditions, the system identifies areas requiring laser ablation and subsequently determines the optimal ablation path/pattern based on the severity of the rust.

To ensure precise tracking of the laser spot along the predefined ablation path, three laser spot tracking control algorithms have been developed, each tailored to different hardware and environmental conditions:

1. Depth Camera and Structured Environment*:* In this approach, the image transmission module is a camera that provides depth information, enabling the internal cavity environment to be treated as a structured environment. The spatial coordinates of the desired ablation path point are known and are represented as P_d^C in the camera coordinate system. The rotation matrix from the camera frame to the mirror frame is denoted as ${}_M^C P$, and the position of the origin of the camera frame relative to the mirror frame is represented by the vector ${}_M^C T$. The coordinates of the desired ablation path point in the mirror frame can be expressed as:

$$P_d^M = {}_M^C P \cdot P_d^C + {}_M^C T = [x_d^M \quad y_d^M \quad z_d^M] \tag{1}$$

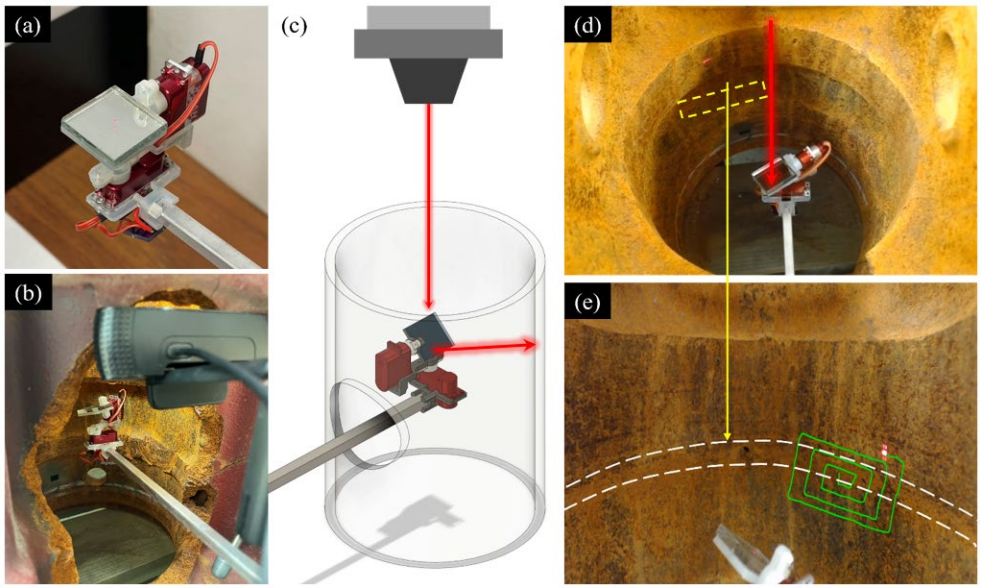

Fig. 2: Experimental setup of the robotic mirror reflective laser scanning control system. (a) The 3D gimbal mechanism. (b) The system positioned within the cavity. (c) Schematic diagram illustrating the system's operation. (d) Top view of the system during operation. (e) Surface area image analysis provided by the image transmission module and laser scanning (The green line indicates the real-time trajectory or pattern of the controlled laser scanning).

Assuming the laser beam is incident vertically on the center of the mirror, to reflect the laser spot onto the desired ablation point, the mirror must rotate by an angle θ_x^M around the x-axis and an angle θ_z^M around the z-axis. Using geometric relationships, the rotation angles θ_x^M and θ_z^M of the mirror can be derived based on the desired reflection:

$$\theta_x^M = \frac{\arccos(z_d^M/\|P_d^M\|)}{2}, \theta_z^M = \arctan2(x_d^M, y_d^M) \quad (2)$$

In general, the camera is fixed directly behind the mirror, so ${}_M^C P = I$, where I represents the identity matrix. When the metal telescopic rod is adjusted to the appropriate position and fixed, ${}_M^C T$ becomes a constant vector. The calculated rotation angles θ_x^M and θ_z^M are then used as rotation angle commands for the two motors in the 3D gimbal mechanism.

***2. Monocular Camera and Structured Environment**:* Depth cameras are typically large, making them unsuitable for smaller-diameter cavities where only compact monocular cameras can be employed. In scenarios where monocular cameras, which lack depth information, are used in unstructured environments, an improved visual servo closed-loop control can be applied to the laser spot tracking task. This visual servo control method consists of two main steps. The first step utilizes a position-based image visual servo approach to reflect the laser spot onto the initial point of the desired path. The camera's intrinsic matrix maps 3D points in the camera coordinate system to 2D pixel coordinates as follows: $P = K \cdot P^C$, where P is the pixel position and P^c is the 3D point in the camera frame. Since position-based image visual servo control requires accurate knowledge of the camera's extrinsic parameters, the extrinsic parameters at the initial point of the path can be determined through camera calibration [13]. However, obtaining the extrinsic parameters for all points along the path would necessitate repeated calibration, which is impractical. Given the relatively smooth surface inside the cavity, it is assumed that a small area around the laser spot forms a smooth plane parallel to the camera. As a result, an image-based visual servo method can be applied to control the laser spot to track the desired path points. The error between the current and desired laser spot positions in the image plane is given by $e_u = u_d - u$ and $e_v = v_d - v$, where $[u, v]$ represents the current pixel position of the laser spot, and $[u_d, v_d]$ represents the target pixel position. To correct these errors, an image-based visual-servo controller is used to adjust the mirror's rotation angles:

$$\theta_x(t) = K_p e_v + K_i \int_0^t e_v(\tau)\, d\tau + K_d \frac{de_v}{dt}$$
$$\theta_z(t) = K_p e_u + K_i \int_0^t e_u(\tau)\, d\tau + K_d \frac{de_u}{dt} \quad (3)$$

where K_p, K_i and K_d are the proportional, integral, and derivative control gains, respectively.

***3. Monocular Camera and Unstructured Environment**:* In cavities where camera calibration is not feasible or in cases involving complex structures where the internal geometry cannot be modeled, a neural network-based ablation path tracking algorithm is proposed and developed. The first step involves performing a low-power laser scan across the entire region to record all mirror angles $[\theta_x, \theta_z]$ and the corresponding laser spot pixel coordinates $[u, v]$, without causing damage to the surface. This scan generates a dataset of input-output pairs, where the pixel coordinates $[u, v]$ serve as the input, and the mirror angles $[\theta_x, \theta_z]$ are the output. The neural network is designed to model the relationship between the pixel coordinates and the mirror angles. The network typically consists of an input layer that accepts the normalized pixel coordinates $[u, v]$, hidden layers with activation functions such as ReLU or tanh to capture the nonlinear relationships, and an output layer that predicts the mirror angles $[\theta_x, \theta_z]$. The network is trained using a mean squared error (MSE) loss function, which minimizes the discrepancy between the predicted and actual mirror angles [14]. Optimizers such as Adam [15] or stochastic gradient descent (SGD) [16] are employed to update the network weights during training. The dataset is split into training and validation sets to ensure the model's ability to generalize. During training, the prediction error is iteratively reduced until the model converges. Once trained, the neural network is deployed within the control system. During operation, the pixel coordinates of the real-time laser spot are input into the network, which predicts the corresponding mirror angles $[\theta_x, \theta_z]$. These predicted angles are then used to adjust the mirror via the 3D gimbal mechanism, ensuring precise control of the laser spot to track the desired positions.

5. Discussion

5.1. Corrosion removal using laser ablation

Fig. 3 demonstrates the effectiveness of laser remanufacturing to remove corroded surfaces from light-level corrosion samples. **Fig. 3a** are images of the samples before and after laser ablation at 0.4 GW/cm² with OR of 50% and 75%. The pre-processed surfaces exhibit extensive rust and oxidation, characterized as 100% corrosion level. Post-processing images reveal significantly reduced corrosion, with the surface appearing much smoother and cleaner, especially at 75% overlap. The higher overlapping ratio provides better coverage and more uniform ablation, leading to a more effective removal of corrosion and restoration of surface quality. Moreover, **Fig. 3b** illustrates optical corrosion percentages as affected by laser intensities (0.2, 0.4, or 0.6 GW/cm²) and OR (25%, 50%, or 75%). The data show that both higher laser intensities and greater overlapping ratios result in a significant reduction in the optical corrosion percentage. At 0.2 GW/cm², the corrosion removal is less effective, as indicated by higher residual corrosion percentages across all overlapping ratios. At 0.4 and 0.6 GW/cm², more corroded materials are removed, with 0.4 GW/cm² achieving a balance between efficient material removal and surface quality, particularly at an OR of 75%. The influence of overlapping ratio is evident across all intensities, with higher overlap ratios yielding more uniform ablation and better corrosion removal. The lowest optical corrosion percentage is observed at 0.4 GW/cm² with a 75% overlap, indicating the optimal combination of laser parameters for light-level corrosion removal.

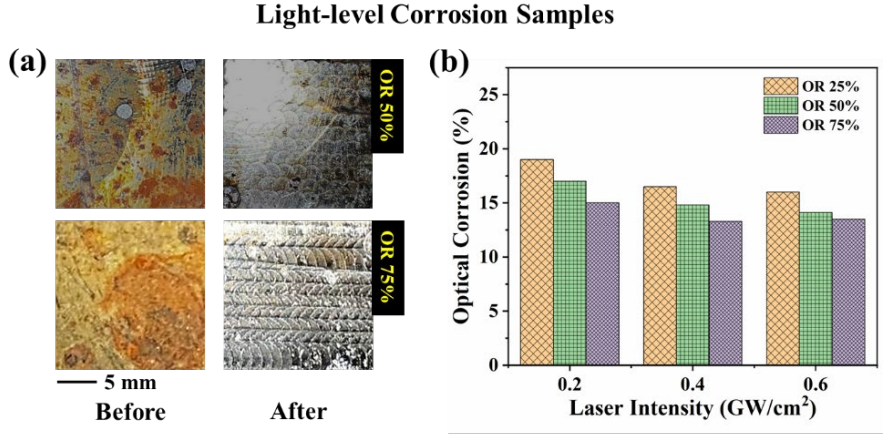

Fig. 3: Corrosion removal of light-level corrosion samples. (a) Images before and after processing at 0.4 GW/cm²; and (b) optical corrosion at various laser intensities and ORs.

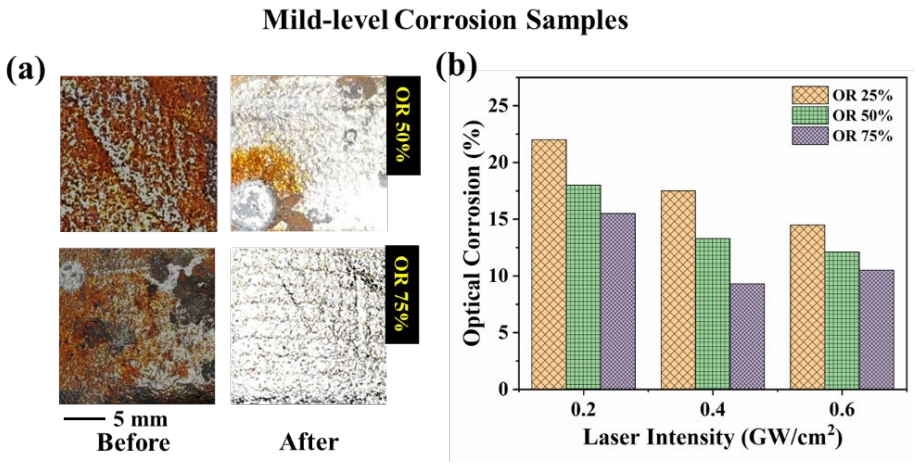

Fig. 4: Corrosion removal of mild-level corrosion samples. (a) Images before and after processing at 0.4 GW/cm^2; and (b) optical corrosion at various laser intensities and ORs.

Fig. 4 highlights the performance of the laser remanufacturing technique for mild-level corrosion samples, revealing distinct insights into the effect of laser parameters on corrosion removal. **Fig. 4a** shows that at 0.4 GW/cm², the surface condition improves significantly after processing, particularly at a 75% OR. While both 50% and 75% ORs reduce visible corrosion, the 75% OR results in a notably smoother and more uniform surface, with minimal residual corrosion. **Fig. 4b** reveals that at higher laser intensities (0.4 and 0.6 GW/cm²), the optical corrosion percentage decreases substantially, confirming the greater efficiency of these intensities in removing corrosion. At 0.4 GW/cm² with a 75% OR, the optical corrosion percentage is at its lowest, suggesting this combination as optimal for mild-level corrosion. Notably, at a 25% OR, the corrosion removal remains less effective across all intensities, emphasizing the critical role of OR in achieving uniform ablation. These results underscore that while both laser intensity and OR are important, the efficiency of laser remanufacturing benefits from a balanced combination of processing parameters, where 0.4 GW/cm² and 75% OR achieve the best corrosion removal while maintaining surface quality.

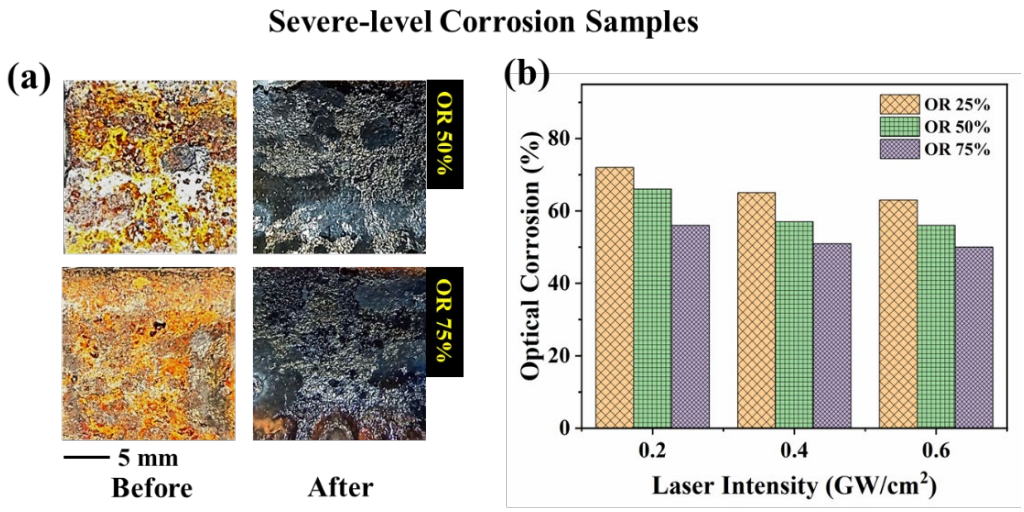

Fig. 5: Corrosion removal of severe-level corrosion samples. (a) Images before and after processing at 0.4 GW/cm^2; and (b) optical corrosion at various laser intensities and ORs.

Fig. 5 demonstrates the effectiveness of the laser remanufacturing technique in addressing severe-level corrosion samples, characterized by thick rust layers and significant surface damage. **Fig. 5a** provides images of corrosion removal at a laser intensity of 0.4 GW/cm² for ORs of 50% and 75%. The pre-processed surfaces show heavy rust buildup and pronounce surface irregularities. Post-processing images reveal a partial reduction in corrosion, with more noticeable improvements at a 75% OR. However, even at 75% OR, residual corrosion and surface roughness remain, highlighting the limitations of laser ablation in fully restoring heavily corroded surfaces. Furthermore, **Fig. 5b**

quantifies the optical corrosion percentages across laser intensities (0.2, 0.4, or 0.6 GW/cm²) and ORs (25%, 50%, or 75%). The results show that higher laser intensities and ORs reduce corrosion. However, even at 0.6 GW/cm² and a 75% OR, the optical corrosion percentage remains higher than those seen in light- and mild-level corrosion scenarios, reflecting the more persistent nature of severe corrosion. At 0.2 GW/cm², the corrosion removal is minimal, regardless of overlap, suggesting insufficient energy for material removal. At 0.4 and 0.6 GW/cm², a 75% OR yields the lowest optical corrosion percentages, though the reductions are less dramatic compared to light- and mild-level samples. These findings indicate that for severe-level corrosion samples, multiple laser scanning cycles on the same location are required for fully remanufacturing of metal surfaces.

In this study, we mainly focused on assessing the capability and effectiveness of pulse laser ablation technique for light to severe level corrosion and coating removal; however, a more detailed investigation on ablation depth and surface morphology before and after processing remains an interesting area for future study. In the following work, we plan to conduct a quantitative investigation to evaluate corrosion ablation depth and determine the effectiveness of multi-pulse ablation process to completely remove severe level corrosion. In addition, further studies will optimize the processing parameters of multi-pulse ablation to efficiently repair components while preserving structural integrity and examine the possible microstructural variation induced during the laser interactions. Our future efforts in this area will provide a deeper understanding of the impacts of laser ablation for the surface repair of severely corroded metallic components, developing an efficient and industrially scalable remanufacturing process.

5.2. Coating removal using laser ablation

Fig. 6 demonstrates the effectiveness of laser remanufacturing for coating removal on a cast iron part. **Fig. 6** compares the original coated part with processed surface at a laser intensity of 0.4 GW/cm², across three ORs of 25%, 50%, or 75%. **Fig. 6a** shows the original part with its intact coating, highlighting the initial surface condition before laser ablation. The coating appears uniform, providing a baseline for evaluating the removal efficiency of the laser processing. **Fig. 6b** illustrates the coating removal results at 0.4 GW/cm². At a 25% OR, the coating is almost completely removed, with minimal residual material observed. However, the surface appears slightly rough and lacks the shininess observed at higher ORs. As the OR increases to 50% and 75%, the surface becomes progressively shinier and more uniform. This indicates that while a 25% OR is sufficient for coating removal, higher ORs contribute to enhanced surface quality by ensuring more uniform ablation and polishing of the underlying material.

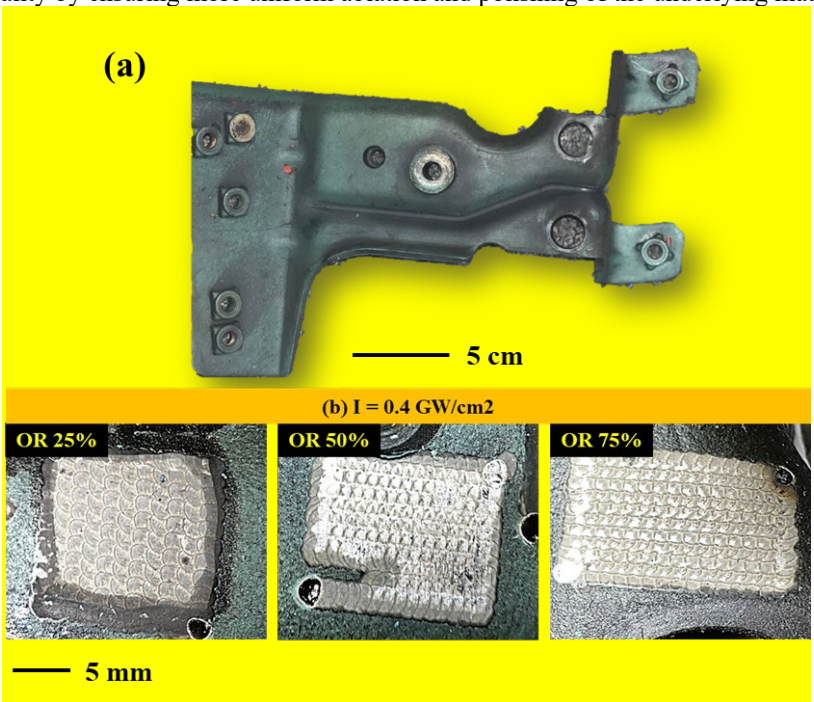

Fig. 6: Removal of surface coatings using laser remanufacturing technique. (a) original part; and (b) processed at 4 GW/cm².

5.3. Robotic mirror reflective laser scanning control results

After setting up the mirror reflective laser scanning control system, the verification of the laser spot tracking control algorithms proposed in Section 2.3 is conducted. The first algorithm, designed for the Depth Camera and Structured Environment, operates in a purely open-loop fashion, with its control accuracy being solely dependent on the precision of the hardware system. As a result, the verification experiment for this algorithm holds limited significance. This section primarily focuses on verifying the algorithms developed for the second and third conditions.

The second algorithm, which operates under the conditions of a Monocular Camera and Structured Environment, requires camera calibration and a relatively smooth surface. To effectively assess the tracking error, the desired ablation path/pattern is defined as a circle and a square on a calibrated plane. The experimental results for this algorithm are presented in **Fig. 7**.

Fig. 7a demonstrates the laser ablation path tracking performance, where the actual ablation path (represented by the red trajectory) closely follows the desired circular path (green trajectory) with a line width of 0.15 cm. The system successfully completes three rotations, maintaining consistent operation. The maximum deviation between the actual and desired paths is approximately 0.07 cm, indicating a satisfactory level of accuracy in the process. In addition, **Fig. 7b** illustrates the laser spot's performance in tracking a non-smooth path. When the desired ablation trajectory is a square, sharp discontinuous vertices appear at the corners. Experimental results show that the two-step visual servo method, as outlined in Section 2.3, allows the laser spot to effectively track such discontinuous paths. However, it is evident that the tracking error increases at the corners, with a maximum deviation of approximately 0.1 cm. Moreover, **Figs. 7c–7e** present the experimental results of the Zigzag pattern scanning. These results indicate that by adjusting the mirror's rotation, the laser spot can systematically cover the entire area to be ablated, with a controllable scanning density. In **Fig. 7e**, it is observed that the error in certain areas is relatively large. This can be attributed to the image recognition algorithm's inability to accurately detect the laser spot in those regions, resulting in imprecise feedback. Since improving the image recognition algorithm is outside the scope of this study, future work will focus on addressing these issues. The results presented demonstrate that the pattern scanning intervals can be finely adjusted from 0.89cm to 0.28cm. To achieve sufficiently small intervals or high-density laser scanning, the integration of a high-precision servo motor along with an advanced control unit will be essential in future work. This improvement will enhance the system's performance and ensure the required level of accuracy.

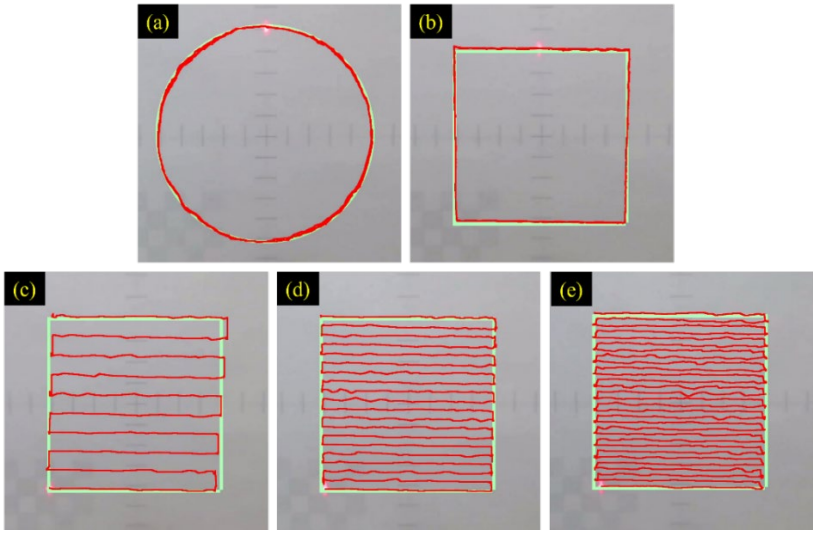

Fig. 7: The experimental results for the Monocular Camera and Structured Environment are shown, with the red line representing the trajectory of the laser spot. The following scenarios are presented: (a) Circular desired ablation trajectory. (b) Square desired ablation trajectory. (c) Zigzag pattern scanning in a square area with an interval of 0.89 cm. (d) Zigzag pattern scanning with an interval of 0.42 cm. (e) Zigzag pattern scanning with an interval of 0.28 cm.

Next, the algorithm under the Monocular Camera and Unstructured Environment condition is validated. The mirror reflective laser scanning control system is set up inside a Volvo engine block inner cavity with unknown dimensions and an unstructured internal environment. Using the network-based ablation path tracking algorithm, the experimental results are presented in **Fig. 8.**

Fig. 8a shows the pre-scanned path, where mirror rotation angle data and laser spot pixel coordinate data are collected. After training the neural network with these two datasets, the desired path (white line in **Fig. 8b**) is provided, and the trained neural network is used to control the laser spot in tracking the desired ablation trajectory. **Fig. 8b** illustrates the tracking results, demonstrating that the trained neural network effectively controls the mirror angles, enabling the laser spot to follow the desired non-smooth ablation path. The laser spot tracking error is smaller near the center of the image, with a maximum deviation of approximately 0.13 cm. However, the tracking error is larger near the edges of the image, with a maximum of approximately 0.32 cm. This discrepancy occurs because the curvature of the pipeline changes more significantly near the edges relative to the pixel variations, resulting in larger errors in the neural network's predictions. In addition, **Figs. 8c** and **8d** present a simulated ablation method. Initially, large-scale ablation is performed, followed by more precise ablation of the local areas that have not been fully cleared. As shown in **Fig. 8c**, the network-based ablation path tracking algorithm can perform ablation in an unstructured environment in a manner similar to the structured environment approach demonstrated in **Fig. 7**. The density of the ablation path can be controlled, and as indicated by the green line in **Fig. 8c**, the local ablation remains within the defined boundary (black-line zone), ensuring precise control during the ablation process.

The effectiveness of the proposed system is validated through two key experiments. First, the laser mirror reflective system significantly enhances ablation accuracy. Traditional laser ablation systems are bulky, making precise position control challenging. In contrast, the proposed system employs the angular adjustment of a compact, lightweight laser reflective mirror system rather than direct positional control of the laser source, reducing complexity while improving stability and precision. As shown in **Fig. 8**, despite the laser being positioned 1.2 m from the ablation area, the final measurement error was only 0.32 cm, demonstrating high accuracy. Second, the system improves ablation speed. With a rotational speed of 154 rad/s, the mirror system enables rapid and efficient ablation due to its high flexibility. Finally, the system expands the ablation workspace and increases operational degrees of freedom, enabling precise ablation on complex surfaces and in confined environments while minimizing blind spots. In the experiment shown in **Fig. 8**, variations in pipeline diameters caused occlusions in lower regions due to smaller-diameter pipes (highlighted in the gray dashed-line area in **Fig. 2e**). The proposed mirror reflective system effectively mitigated these blind spots, demonstrating its adaptability to constrained environments.

In summary, the presented results demonstrate the superior performance of the developed laser scanning system and control methods. The system effectively controls the laser spot for laser remanufacturing purposes, particularly for processing engineering components with complicated internal and external features.

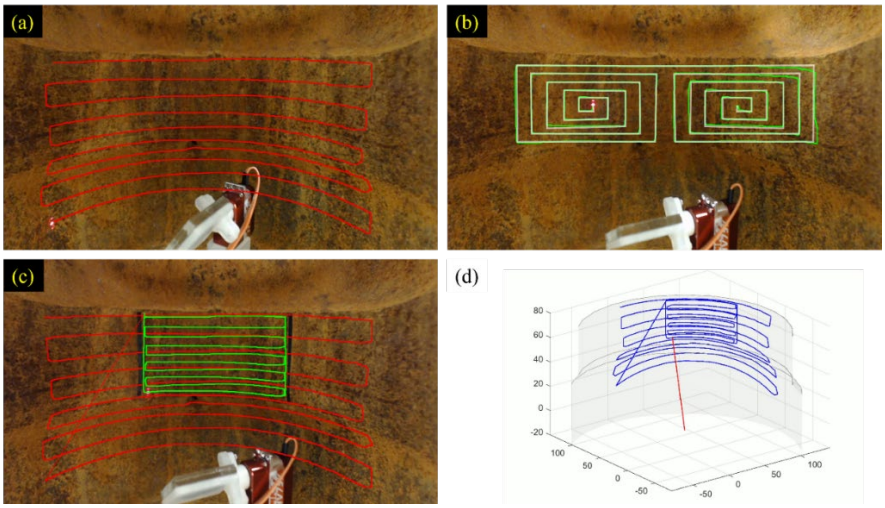

Fig. 8: The experimental results that validate the Monocular Camera and Unstructured Environment approach.

6. Conclusions & Recommendations

In this work, a novel remanufacturing technology, laser surface ablation, was developed to remove surface corrosion and coating of metallic components. The laser remanufacturing technology was evaluated using cast iron samples with light-, mild-, severe-corrosion levels. In addition, laser remanufacturing for removing surface coating was investigated. The results demonstrated the exceptional effectiveness and efficiency of laser ablation technology for surface remanufacturing of cast iron components. Parametric study indicated the importance of laser intensity and

OR for laser surface remanufacturing. In addition, robotic mirror reflective laser scanning control system was developed, aiming to evaluate the capability of laser remanufacturing of both external and internal surfaces of engineering components. The proposed laser processing technology is expected to provide an eco-friendly, energy-efficient, highly controllable, and user-friendly solution for metallic surface remanufacturing.

7. Acknowledgements

The authors thank the financial support from REMADE, project number 21-01-RM-5086.

8. References

[1] Zuo, Z.; Hu, R.; Wang, Q.; Gao, Z.; Luo, X.; Lai, Y.; Xue, S.; Xiang, M.; Zhao, X.; Li, S., Effects of Thermal Exposure on the Microstructure and Mechanical Properties of a Ti–48Al–3Nb–1.5Ta Alloy via Powder Hot Isostatic Pressing, *Materials*, vol. 17, 4, 2024.

[2] Basdeki, M., Apostolopoulos, C., The Effect of Shot Blasting Process on Mechanical Properties and Anti-Corrosive Behavior of Steel Reinforcement, *Metals*, vol. 12, 2, 2022.

[3] Öztürk, B., White, E. M. H., Dickes, D., Glatzel, U., Mengis, L., Galetz, M. C., "Improved tribological behavior of Ti-6Al-4V through a novel zirconium diffusion coating, Surf. Coat. Tech., vol. 487, p. 130993, 2024.

[4] Deng, J., Zhao, G., Lei, J., Zhong, L., Lei, Z., Research Progress and Challenges in Laser-Controlled Cleaning of Aluminum Alloy Surfaces, *Materials*, vol. 15, 16, 2022.

[5] Li, X., Huang, T., Chong, A. W., Zhou, R., Choo, Y. S., Hong, M., Laser cleaning of steel structure surface for paint removal and repaint adhesion, Optoelectronic Engineering, vol. 44, no. 3, p. 340, 2017.

[6] Rubbi, F., Zhang, X., Delzendehrooy, F., Mao, B., Nian, Q., Doumanidis, C., Liao, Y., Chemical etching enhanced nanosecond pulsed laser micromachining: An experimental and numerical investigation, J. Manuf. Process., 108, 384-394, 2023.

[7] Liao, Y., Yang, Y., Cheng, G., Enhanced laser shock by an active liquid confinement -hydrogen peroxide, ASME J. Manuf. Sci. Eng., 134, 3, 2012.

[8] Zhang, Z., Nian, Q., Doumanidis, C., Liao, Y., First-principles modeling of laser-matter interaction and plasma dynamics in nanosecond pulsed laser shock processing, J. Appl. Phys., vol. 123, 5, 2018.

[9] Medeiros, F. N. S., Ramalho, G. L. B., Bento, M. P., Medeiros, L. C. L., On the Evaluation of Texture and Color Features for Nondestructive Corrosion Detection, J. Adv. Signal Process., 2010, 1, 2010.

[10] Naik, D. L., Sajid, H. U., Kiran, R., Chen, G., Detection of Corrosion-Indicating Oxidation Product Colors in Steel Bridges under Varying Illuminations, Shadows, and Wetting Conditions, Metals, 10, 11, 2020.

[11] Ramírez Barat, B., Cano, E., Molina, M. T., Barbero-Álvarez, M. A., Rodrigo, J. A., Menéndez, J. M., Design and Validation of Tailored Colour Reference Charts for Monitoring Cultural Heritage Degradation, Herit. Sci., 9, 1, 2021.

[12] Cui, K., Luo, J., Xu, K., Ling, L., Cheng, R., The Study of Patterns and Mechanisms of Continuous Laser Ablation of Carbon Steel Rust Layers in Multi-Medium Environments, Appl. Sci., 14, 12, 2024.

[13] Hutchinson, S., Hager, G. D., Corke, P., A Tutorial on Visual Servo Control, IEEE T-RA., 12, 5, 1996.

[14] Dongare, D., Kharde, R. R., Kachare, A. D., Introduction to Artificial Neural Network, Int. J. Eng. Innov. Technol., 2, 1, 2012.

[15] Jais, Ismail, A., Nisa, S., Adam Optimization Algorithm for Wide and Deep Neural Network, Knowledge Engineering and Data Science, 2, 1, 2019.

[16] Bottou, L., Stochastic Gradient Descent Tricks, Neural Networks: Tricks of the Trade: Second Edition. Berlin, Heidelberg, pp. 421-436, Springer, 2012.

9. About the Authors

Fazlay Rubbi, PhD students at Iowa State University (ISU) with research focus on laser manufacturing.
M. Merajul Haque, PhD students at ISU with research focus on laser manufacturing.
Liuyin Wang, PhD student at University of Nevada Reno with research focus on mirror reflective robotic control.
Dr. Beiwen Li, associate professor at University of Georgia with expertise in surface characterization.
Dr. Yantao Shen, professor at UNR with expertise in sensor based robotic control.
Dr. Gül E Kremer, professor at University of Dayton with expertise in advanced manufacturing.
Dr. Yiliang Liao, associate professor at ISU with expertise in laser manufacturing.